Supporting Information for:

Orbital energy mismatch engenders high-spin ground states in heterobimetallic complexes

Scott C. Coste[a], Tyler J. Pearson[a], Alison B. Altman[a], Ryan A. Klein[a], Brian Finney[b], Michael Y. Hu[c], E. Ercan Alp[c], Bess Vlaisavljevich[b], Danna E. Freedman[a]*

[a] *Department of Chemistry, Northwestern University, Evanston, Illinois 60208*
[b] *Department of Chemistry, University of South Dakota, Vermillion, South Dakota 57069*
[c] *Advanced Photon Source, Argonne National Laboratory, Lemont, IL, 60439*

Table of Contents:

Experimental Details **S4**

Table S1 | Crystallographic information of **1** **S11**

Table S2 | Crystallographic information of **2** **S12**

Table S3 | Crystallographic information of **3** **S13**

Table S4 | Crystallographic information of **4** **S14**

Table S5 | Crystallographic information of **6** **S15**

Table S6 | Crystallographic information of **7** **S16**

Table S7 | Tabulated ^{57}Fe Mössbauer parameters **S17**

Table S8 | Spin Hamiltonian parameters from fitting Magnetization data **S17**

Table S9 | Simulation parameters for EPR spectra of **1** and **3** **S17**

Table S10 | Peak-fitting results for XAS data **S18**

Table S11 | Fitted parameters for ^{119}Sn SMS data **S18**

Table S12 | Atomic charges from DFT calculations **S19**

Table S13 | Atomic spin densities from DFT calculations **S19**

Table S14 | Bond orders from DFT and CASSCF calculations **S20**

Table S15 | Occupation and effective bond orders of σ-bond from CASSCF **S20**

Table S16 | Orbital decomposition from DFT calculations **S21**

Table S17 | Hirshfeld atomic Sn contributions to CASSCF orbitals **S21**

Table S18 | Hirshfeld atomic transition metal contributions to CASSCF orbitals **S22**

Table S19 | Sn and transition metal s/p/d contributions to metal-metal bond **S22**

Table S20 | Calculated spin Hamiltonian parameters **S23**

Table S21 | Experimental and calculated spin-allowed electronic excited state energies **S23**

Figure S1 | Powder X-Ray diffraction patterns for **3** – **7** **S24**

Figure S2 | Raman spectra for **3** – **7** **S25**

Figure S3 | Electronic absorption spectra of **3**, **4**, and **6** in C_6D_6 **S26**

Figure S4 | Zoomed in diffuse reflectance spectrum of **3** **S27**

Figure S5 | Plot of MMCT band energy against transition metal electronegativity **S28**

Figure S6 | Variable-field magnetization of **3**, **4**, and **6** at 100 K **S29**

Figure S7 | Variable-field, variable temperature magnetization of **3** **S30**

Figure S8 | EPR spectra of **1** and **3** at various temperatures **S31**

Figure S9 | XANES data for reference compounds and 1st derivative plots **S32**

Figure S10 | Plot of ^{119}Sn ΔE_Q values against axial ligand electronegativity **S33**

Figure S11 | Active natural orbitals from CASSCF calculations for **3** **S34**

Figure S12 | Active natural orbitals from CASSCF calculations for **4** **S35**

Figure S13 | Active natural orbitals from CASSCF calculations for **5** **S36**

Figure S14 | Active natural orbitals from CASSCF calculations for **6** **S37**

References **S38**

Experimental Details.

General Considerations. All compounds were manipulated and handled under a dinitrogen atmosphere in an MBraun Unilab Pro glovebox. All glassware was either oven-dried at 150 °C for at least four hours or flame-dried prior to use. Dichloromethane (DCM), methanol (MeOH), Diethylether (Et_2O), benzene, toluene, and n-hexane were dried using a commercial solvent purification system from Pure Process Technology and stored over 3 or 4 Å sieves for a minimum of one day prior to use. $CDCl_3$ and C_6D_6 were purchased from Cambridge Isotope Labs, deoxygenated by three successive freeze-pump-thaw cycles, filtered through a pad of activated alumina, and stored over 3 or 4 Å sieves prior to use. $KTp^{Ph,Me}$, $^{Ph,Me}TpFeCl$, $^{Ph,Me}TpCoCl$, and $[^{Ph,Me}TpNiCH_2SiMe_3]\cdot\frac{1}{2}$ hexane, and $[^{Ph,Me}TpCoSnPh_3]$ were prepared according to literature procedures.[1–5] $HSnPh_3$ was purchased from MilliporeSigma and vacuum distilled prior to use. All other chemicals were used as received. Silylated Celite was prepared by stirring 25 g activated, dried Celite 545 in 100 mL toluene with 14 mL trimethylsilylchloride and 14 mL of triethylamine under N_2 overnight at 40 °C, followed by filtration, washing with 80 mL MeOH and 200 mL toluene, and drying for 24 hours at 100 °C.

$[^{Ph,Me}TpMnCl]$(1). A solution of KTp (1.0463 g, 2.00 mmol) in 15 mL DCM was added to a stirring solution of $MnCl_2$ (0.2573 g, 2.04 mmol) in 3 mL MeOH at room temperature. The white, cloudy solution was allowed to stir overnight at room temperature. The reaction mixture was subsequently pumped down to dryness. The product was extracted into 20 mL DCM, filtered through a Celite pad on a fritted filter, and then concentrated to about 4 mL. Crystalline product suitable for X-ray diffraction was obtained by adding 15 mL of n-hexane and allowing it to sit at room temperature overnight. The white needles were then isolated by decanting the mother liquor, washing with 3 x 5 mL n-hexane, and drying *in vacuo*. Yield: 0.4563 g (39.7%). IR (ATR, cm^{-1}): 3131 (w), 3057 (w), 2968 (w), 2927 (w), 2909 (w), 2570 (w), 1577 (w), 1570 (w), 1558 (w), 1541 (m), 1521 (w), 1507 (m), 1497 (w), 1486 (m), 1478 (m), 1464 (w), 1456 (w), 1450 (m), 1431 (m), 1410 (m), 1400 (w), 1387 (w), 1379 (w), 1357 (m), 1341 (m) , 1323 (m), 1304 (m), 1282 (w), 1188 (m), 1172 (m), 1156 (m), 1106 (m), 1096 (m), 1067 (s), 1041 (m), 1030 (w), 999 (w), 993 (w), 977 (m), 913 (m), 842 (w), 827 (w), 799 (m), 778 (s), 761 (vs), 690 (vs), 679 (vs), 668 (s), 658 (m), 640 (s), 619 (m), 603 (m). Anal. Calcd. for $MnClN_6C_{30}BH_{28}$: 62.80 %C; 4.92 %H; 14.65 %N. Found: 62.70 %C; 4.83 %H; 14.53 %N.

[^{Ph,Me}TpZnCl](2). A solution of KTp (1.3216 g, 2.53 mmol) in 15 mL DCM was added to a stirring solution of $ZnCl_2$ (0.3483 g, 2.56 mmol) in 3 mL MeOH at room temperature. The white, cloudy solution was allowed to stir overnight at room temperature. The reaction mixture was subsequently pumped down to dryness. The product was extracted into 20 mL DCM, filtered through a Celite pad on a fritted filter, and then concentrated to about 4 mL. Crystalline product suitable for X-ray diffraction was obtained by adding 15 mL of n-hexane and allowing it to sit at room temperature overnight. The white needles were then isolated by decanting the mother liquor, washing with 3 x 5 mL n-hexane, and drying *in vacuo*. Yield: 0.6667g (45.1%) IR (ATR, cm^{-1}): 3139 (w), 3122 (w), 3089 (w), 3061 (w), 3046 (w), 3027 (w), 2988 (w), 2961 (w), 2930 (w), 2916 (w), 2546 (m), 1574 (w), 1568 (w), 1545 (m), 1508 (w), 1474 (m), 1438 (m), 1414 (m), 1385 (m), 1370 (m), 1342 (m), 1310 (w), 1282 (w), 1216 (w), 1186 (m), 1171 (s), 1129 (w), 1094 (m), 1064 (s), 1028 (w), 998 (w), 984 (m), 917 (w), 909 (w), 858 (w), 836 (w), 810 (m), 804 (m), 781 (m), 772 (m), 759 (vs), 721 (w), 704 (m), 691 (vs), 668 (m), 655 (m), 636 (s), 623 (w), 616 (w), 612 (w), 604 (w). ^{1}H NMR (500 MHz, $CDCl_3$, 298 K): δ 7.72 (d, 6H), 7.41 (t, 6H), 7.36 (t, 3H), 6.26 (s, 3H), 5.00 (br d, 1H), 2.57 (s, 9H) ppm. Anal. Calcd. for $ZnClN_6C_{30}BH_{28}$: 61.68 %C; 4.83 %H; 14.38 %N. Found: 61.46 %C; 4.91 %H; 14.17 %N.

[^{Ph,Me}TpMnSnPh$_3$]·benzene(3). Yellow $KSnPh_3$ was generated by stirring $HSnPh_3$ (482.0 mg, 1.373 mmol) and KH (55.1 mg, 1.374 mmol) in 5 mL of Et_2O for 4 hours at room temperature. To this, a suspension of **1** (504.0 mg, 0.8784 mmol) in 15 mL Et_2O was added at room temperature, a white precipitate formed and the reaction was allowed to stir overnight at room temperature. The precipitate was filtered out and washed with 4 x 5 mL Et_2O and dried. Then, it was taken up in 80 mL benzene, filtered through silylated Celite on a fritted funnel, then layered under 100 mL n-hexane. Colorless hexagonal platelets of **3** were obtained (Yield: 410.5 mg, 48.4%). The IR (ATR, cm^{-1}): 3048 (w), 3023 (w), 3001 (w), 2975 (w), 2964 (w), 2928 (w), 2527 (w), 1542 (m), 1506 (w), 1474 (m), 1450 (m), 1432 (s), 1423 (s), 1376 (w), 1358 (m), 1341 (m), 1303 (w), 1283 (w), 1254 (w), 1215 (w), 1178 (s), 1092 (m), 1060 (s), 1030 (m), 995 (w), 975 (m), 912 (w), 841 (w), 802 (w), 777 (m), 763 (s), 730 (s), 695 (s), 677 (vs), 656 (s), 638 (s), 531 (m), 522 (m), 489 (m), 451 (s), 442 (s), 409 (w). UV-Vis-NIR (C_6D_6) λ_{max}, nm (ε): 360 (2595). Anal. Calcd. for $SnMnN_6C_{48}BH_{43}\cdot{}^1/_2(C_6H_6)$: 66.04 %C; 5.00 %H; 9.06 %N. Found: 66.34 %C; 5.01 %H; 8.83 %N.

[^{Ph,Me}TpFeSnPh$_3$]·benzene(4). **4** was synthesized in a similar fashion to **3**, except that [^{Ph,Me}TpFeCl] (510.3 mg, 0.8879 mmol) was reacted with KSnPh3 (1.373 mmol). Orange, hexagonal platelets of **4** were obtained with a benzene/n-hexane layering (Yield: 295.9 mg, 34.4 %). IR (ATR, cm^{-1}): 3048 (w), 3024 (w), 2995 (w), 2975 (w), 2965 (w), 2919 (w), 2527 (w), 1541 (m), 1506 (w), 1474 (m), 1451 (m), 1433 (s), 1423 (s), 1376 (w), 1359 (m), 1342 (m), 1300 (w), 1285 (w), 1254 (w), 1214 (w), 1180 (s), 1093 (m), 1058 (s), 1030 (m), 995 (w), 976 (m), 912 (w), 841 (w), 802 (w), 776 (m), 763 (s), 730 (s), 696 (s), 677 (vs), 656 (s), 637 (s), 532 (m), 524 (m), 488 (m), 451 (s), 442 (s), 417 (w). UV-Vis-NIR (C_6D_6) λ_{max}, nm (ε): 356 (1331), 462 (1510), 513 (sh, 727). ^{1}H NMR (500 MHz, C_6D_6, 298 K): δ 59.90 (3H), 32.59 (6H), 29.33 (9H), 10.20 (6H), 8.86 (3H), 7.67 (6H), 6.29 (3H), 5.85 (6H), -15.79 (1H) ppm. Anal. Calcd. for $SnFeN_6C_{48}BH_{43}\cdot(C_6H_6)$: 67.05 %C; 5.11 %H; 8.69 %N. Found: 66.76 %C; 5.07 %H; 8.41 %N.

[^{Ph,Me}TpNiSnPh$_3$]·benzene(6). A solution of $HSnPh_3$ (107.0 mg, 0.3048 mmol) in 2 mL of n-hexane was added to a stirring solution of [^{Ph,Me}TpNiCH$_2$SiMe$_3$]·½ hexane (151.6 mg, 0.2261 mmol) in 15 mL of n-hexane at room temperature. After allowing the reaction mixture to stir for 5 hours at room temperature, the turquoise precipitate was filtered out and washed with 3 x 5 mL hexanes then dried *in vacuo*. Turquoise, hexagonal platelets of **6** were obtained by dissolving the product in 8 mL benzene, filtering through silylated Celite, and layering under 30 mL of n-hexane. (Yield: 107.9 mg, 49.2%) IR (ATR, cm^{-1}): 3048 (w), 3024 (w), 2995 (w), 2975 (w), 2965 (w), 2931 (w), 2521(w), 1543 (m), 1506 (w), 1475(m), 1451 (m), 1435 (s), 1423 (s), 1377 (w), 1361 (m), 1344 (m), 1300 (w), 1285 (w), 1253 (w), 1218 (w), 1186 (s), 1094 (m), 1057 (s), 1031 (m), 996 (w), 979 (m), 912(w), 838 (w), 803 (w), 779 (m), 763 (s), 730 (s), 697 (s), 676 (vs), 656 (s), 637 (s), 535 (m), 528 (m), 488 (m), 452 (s), 443 (s), 404 (w). UV-Vis-NIR (C_6D_6) λ_{max}, nm (ε): 367 (1975), 576 (1511), 709 (1191), 975 (348). ^{1}H NMR (500 MHz, C_6D_6, 298 K): δ 73.93, 14.39, 9.99, 9.55, 8.90, 8.01, 7.47, 7.08, −9.24 ppm. Anal. Calcd. for $SnNiN_6C_{48}BH_{43}\cdot(C_6H_6)$: 66.85 %C; 5.09 %H; 8.66 %N. Found: 66.54 %C; 5.09 %H; 8.82 %N.

[^{Ph,Me}TpZnSnPh$_3$]·benzene (7). **7** was synthesized in a similar fashion to **3**, except that **2** (559.0 mg, 0.9578 mmol) was reacted with $KSnPh_3$ (1.437 mmol). Colorless, hexagonal platelets of **7** were obtained with a benzene/n-hexane layering (Yield: 451.0 mg, 48.3 %). IR (ATR, cm^{-1}): 3050 (w), 3026 (w), 2996 (w), 2977 (w), 2966 (w), 2931 (w), 2513 (w), 1544 (m), 1507 (w), 1476 (m), 1451 (m), 1435 (s), 1424 (s), 1376 (w), 1362 (m), 1343 (m), 1301 (w), 1286 (w) 1255 (w), 1219

(w), 1186 (s), 1093 (m), 1059 (s), 1031 (m), 996 (w), 976 (m), 913 (w), 834 (w), 803 (w), 780 (m), 764 (s), 731 (s), 697 (s), 676 (vs), 656 (s), 637 (s), 532 (m), 527 (m), 489 (m), 451 (s), 443 (s), 410 (w). ^{1}H NMR (600 MHz, C_6D_6, 298 K): δ 7.50 (d, 6H), 7.14 (t, 3H), 7.09 (t, 6H), 7.04 (d, 6H), 6.75 (t, 3H), 6.50 (t, 6H), 5.93 (s, 3H), 5.00 (br s, 1H), 2.24 (s, 9H) ppm. ^{119}Sn NMR (223.8 MHz, C_6D_6, 298 K) −118.45 ppm Anal. Calcd. for $SnZnN_6C_{48}BH_{43}\cdot\frac{1}{2}(C_6H_6)$: 65.31 %C; 4.94 %H; 8.96 %N. Found: 65.39 %C; 4.82 %H; 9.15 %N.

Magnetic Measurements. Magnetic data were collected using a Quantum Design MPMS-XL SQUID magnetometer. Measurements for all compounds were obtained on finely ground microcrystalline powders. The compounds were restrained in a frozen eicosane matrix and flame sealed in a quartz tube under vacuum. Dc susceptibility measurements were collected in the temperature range 1.8–300 K under dc fields of 0.1, 0.5 and 1 T. Dc magnetization measurements were performed under applied magnetic fields of 1, 2, 3, 4, 5, 6 and 7 T in the temperature range of 1.8–10 K. Dc magnetic susceptibility data were corrected for diamagnetic contributions from the sample holder and eicosane as well as for the core diamagnetism of each sample, estimated using Pascal's constants.[6] Prior to full characterization, variable dc field magnetization data was collected from 0 to 4 T at 100 K to ensure the absence of curvature associated with ferromagnetic impurities.

X-ray Diffraction. Single crystal diffraction data collections were performed on single crystals coated with Paratone-N oil and mounted on a MicroMounts^{TM} rod. The crystals were frozen while coated in Paratone-N oil under a stream of N_2 during the measurement. Structures for **1 - 7** were collected with a Mo Kα (λ = 0.71073 Å) sealed tube diffraction source with a graphite monochromator, and a Bruker APEX2 CCD detector. Raw data were integrated and corrected for Lorentz and polarization effects using Bruker Apex3 v. 2013.[7] Absorption corrections were applied using SADABS.[8] Space group assignments were determined by examination of systematic absences, *E*-statistics, and successive refinement of the structures. The crystal structure was solved by direct methods with the aid of successive difference Fourier maps in SHELXS[9] operated with the OLEX2 interface.[10] The crystals showed no significant decay during data collection. Thermal parameters were refined anisotropically for all non-hydrogen atoms. Hydrogen atoms were placed in ideal positions and refined using a riding model for all structures. Compounds **3** – **7** crystallized with a benzene molecule that was disordered over a special position, so a solvent mask was used.

Zero-field ^{57}Fe Mössbauer Spectroscopic Measurements. Measurement of **4** was performed under zero applied magnetic field and at 80 K on ca. 70 mg of ground, microcrystalline product. The sample was loaded into a circular plastic cap of 1 cm^2 area under an inert atmosphere covered in Paratone-N oil and transferred quickly to the cryostat to avoid sample decomposition. The spectrum was collected with a constant acceleration spectrometer and a ^{57}Co/Rh source. Prior to measurements, the spectrometer was calibrated at 295 K with α-Fe foil. Spectra were analyzed using the WMOSS Mössbauer Spectral Analysis Software (www.wmoss.org).

Raman Spectroscopy Measurements. Crystals of **3** – **7** were sealed in 0.7 mm capillaries with Illumabond UV Curable Epoxy in the glovebox. Raman spectra were collected using a Horiba LabRam HR Evolution confocal microscope. Individual crystals were excited with 633 nm (compounds **3** and **4**) and 532 nm (compounds **5** – **7**) continuous-wave diode lasers equipped with a long working distance 50× microscope objective (NA = 0.50; Nikon) and 1800 grooves/mm grating at 0.95 mW (633 nm) and 2.5 mW (532 nm) power at room temperature. The spectra were collected for 10 minutes.

Powder X-ray Diffaction Measurements. Polycrystalline samples of **3** – **7** where loaded in a hollow metallic sample holder and both sides sealed with Kapton tape inside the glovebox. The powder X-ray diffraction (PXRD) patterns were measured in transmission geometry (with sample spinning) using a STOE STADI P instrument equipped with a CuKα1 sealed tube source and a 1D strip detector covering 2θ range of 6°. All patterns were collected at room temperature.

Electron Paramagnetic Resonance (EPR) Spectroscopy. Polycrystalline samples were loaded into a 4 mm OD quartz EPR tube under a dinitrogen atmosphere and restrained with eicosane. Continuous-wave EPR spectra were measured at the University of Chicago EPR facility using a Bruker Elexsys 500 X-band EPR spectrometer. Samples were cooled using an Oxford Systems continuous-flow He cryostat coupled with a 10 K He stinger from Bruker. Spectra were acquired with the Bruker Win-EPR software suite. Spectral simulations were carried out using Easyspin.[11]

X-Ray Absorption Spectroscopy (XAS). Transmission XAS measurements at the Sn K-edge (29.2 keV) were acquired at sector 20-BM at the Advanced Photon Source of Argonne National Laboratory. Samples were prepared by sealing layers of polycrystalline or amorphous powders between pieces of Kapton tape inside a dinitrogen glovebox and adhering the layers to Teflon

sample holders. The sample holders were then mounted onto a sample rod and placed under vacuum. Samples were measured at 25 K using a Displex closed-cycle He refrigerator. All measurements at the Sn K-edge were run concurrently with Sn foil for energy calibration. The spectra were normalized and analyzed using the software Athena.[12]

^{119}Sn Synchrotron Mössbauer Spectroscopy. Spectra for **3** – **7** were measured at Sector 30-ID at the Advanced Photon Source of Argonne National Laboratory. Samples were prepared by mixing unenriched polycrystalline powders with oil, to improve thermal conductivity, and placing inside a custom-made 9-well copper sample holder in a dinitrogen-filled glovebox. Kapton tape was used to seal the samples and protect from dioxygen. Measurements were done under vacuum and cooled used a closed-loop He refrigerator equipped with a Be window. The spectra were fit iteratively with the Newton method using the CONUSS-2.2.0 software. The agreement between data and the fits were parameterized by a normalized χ^2 value which are displayed for each fit in Table S11. The natural abundance of ^{119}Sn was used for fitting with a fixed Lamb-Mössbauer factor of 0.05. The density of each compound was fixed to the value obtained from single crystal X-Ray diffraction measurements. We fit the spectra using a single Sn site and allowed the following parameters to freely refine: ΔE_Q, texture coefficient, sample thickness, and the scaling factor. We used the density obtained from single crystal X-ray diffraction and used a Lamb-Mössbauer factor of 0.05 for the fits. A distribution of electric quadrupole splitting was also used in the fit and allowed to refine freely.

All Other Physical Measurements. Combustion analysis of all complexes was performed by Midwest Microlabs (Indianapolis, IN). Infrared spectra were recorded on a Bruker Alpha FTIR spectrometer equipped with an attenuated total reflectance accessory. Solution-phase NMR spectra were collected with a Bruker Avance III 600 MHz spectrometer. Proton NMR spectra are referenced to $CDCl_3$ or d_6-benzene at 7.26 and 7.16 ppm, respectively. UV-vis-NIR and diffuse reflectance spectra were collected on a Varian Cary 5000 spectrometer at room temperature in C_6D_6 for the solutions or over KBr for solid measurements.

Computational Details.

Analysis of bonding in the ground state. Single point energy calculations were performed for molecular geometries obtained from experiment using density functional theory (DFT) to analyze

the bonding in **3-7** and compare with the CASPT2 results. All calculations were performed in the Turbomole program package.[13] The TPSSh[14,15] functional and def2-TZVP basis set[16] was used. The resolution of the identity (RI) approximation was used as well.[17–19] Atomic charges, spin densities, and the charge decomposition of the σ bonding orbital computed using intrinsic bond orbital (IBO) analysis as implemented in IboView.[20] Mayer bond orders were computed using the MultiWFN program.[21,22] The occupation numbers for the lowest CI Root from the CASSCF calculation described above (for the ground state spin) were used to calculate the so-called effective bond order (EBO) which is the occupation number of the bonding orbital minus the occupation number of the antibonding orbital, divided by two.

Calculated Magnetic Properties. All complete active space self-consistent field level of theory (CASSCF) with corrections to the energy from second order perturbation theory (CASPT2) were performed on geometries obtained by diffraction experiments for **3-6**.[23–25] The active space includes the 3d and 4d orbitals from the transition metal (Mn, Fe, Co, or Ni) along with the bonding and antibonding orbitals between Sn and transition metal. The corresponding number of electrons to maintain a neutral charge were included. Specifically, the active spaces were (7*e*, 12*o*), (8*e*, 12*o*), (9*e*, 12*o*), and (10*e*, 12*o*), for Mn, Fe, Co, and Ni, respectively. All calculations were performed with the OpenMolcas 8.0 software package.[26] An imaginary shift of 0.2 and an IPEA shift of 0.25 were used in all CASPT2 calculations. ANO-RCC basis sets was used for all atoms with the following contractions: 6s5p3d2f1g for Mn, Fe, Co and Ni; 6s5p3e1f for Sn; 3s2p1d for N; 2s1p for B and C; and 1s for H.[27–30] CASPT2 calculations were performed for the lowest energy state of the ground state spins (S=3/2 for Co, S=1 for Ni, and S=2 for Fe) to analyze the bonding. The natural orbitals and their occupation in the spin-free ground state are shown in Figures S11 to S14. The orbitals were state-averaged and all excitations within the 3d manifold were computed. This corresponds to the following number of states: Mn (1 sextet, 24 quartets, and 75 doublets), Fe (5 quintets, 45 triplets, and 50 singlets), Co (10 quartets and 40 doublets), and Ni (10 triplets and 15 singlets). Spin-orbit coupling effects were included *a posteriori* using the restricted active space state interaction approach (RASSI). The diagonal elements of the effective Hamiltonian were replaced with the single state CASPT2 energies. The obtained RASSI spin-orbit states were introduced into the SINGLE-ANISO module to calculate the magnetic properties (*D* and *E*).[31] Additional information regarding the excited state electron configurations can be found at the University of South Dakota's library database via this link: https://red.library.usd.edu/data/1/.

Table S1 | Crystallographic information for the structural refinement of **1**.

Empirical Formula	$MnClN_6C_{30}BH_{28}$
Formula weight	573.78 g/mol
Temperature	100.07 K
Wavelength	0.71073 Å
Crystal System	Trigonal
Space Group	*R*3c
Unit Cell Dimensions	a = 12.0230(1) Å, α = 90.0° b = 12.0230(1) Å, β = 90.0° c = 32.558(3) Å, γ = 120.0°
Volume	4075.8(1) Å^3
Z	6
Density (calculated)	1.403 g/cm^3
Absorption coefficient	0.616 mm^{-1}
F_{000}	1782.0
Crystal color	Colorless
Crystal size	0.342 × 0.150 × 0.084 mm^3
2θ range	4.644 to 68.426°
Index ranges	$-19 \le h \le 18$ $-19 \le k \le 18$ $-21 \le l \le 51$
Reflections collected	41720
Independent reflections	7916 [R_{int} = 0.0371]
Completeness to 2θ = 68.426°	81.1 %
Absorption correction	Multi-scan
Maximum and minimum transmission	0.4853 and 0.4292
Refinement method	Full-matrix least-squares on F^2
Data / restraints / parameters	2860 / 1 / 119
Goodness-of-fit on F^2[a]	1.061
Final R indices [$I > 2\sigma(I)$][b]	R_1 = 3.10 %, wR_2 = 6.80 %
R indices (all data)	R_1 = 4.15 %, wR_2 = 7.18 %
Largest diff. peak and hole	0.31 and –0.36 e.Å^{-3}

[a] GooF = $[\Sigma[w(F_o^2-F_c^2)^2] / (n-p)]^{1/2}$ where n is the number of reflections and p is the total number of parameters refined. [b] $R_1 = \Sigma||F_o|-|F_c|| / \Sigma|F_o|$; $wR_2 = [\Sigma[w(F_o^2-F_c^2)^2] / \Sigma[w(F_o^2)^2]]^{1/2}$

Table S2 | Crystallographic information for the structural refinement of **2**.

Empirical Formula	$ZnClN_6C_{30}BH_{28}$
Formula weight	584.21 g/mol
Temperature	100.11 K
Wavelength	0.71073 Å
Crystal System	Monoclinic
Space Group	$P2_1/n$
Unit Cell Dimensions	a = 11.0364(8) Å, α = 90.0° b = 15.2242(1) Å, β = 94.548(2)° c = 16.1001(1) Å, γ = 90.0°
Volume	2696.6(4) Å^3
Z	4
Density (calculated)	1.439 g/cm^3
Absorption coefficient	1.04 mm^{-1}
F_{000}	1208.0
Crystal color	Colorless
Crystal size	0.348 × 0.122 × 0.040 mm^3
2θ range	3.688 to 60.42°
Index ranges	$-15 \le h \le 15$ $-21 \le k \le 21$ $-22 \le l \le 22$
Reflections collected	44426
Independent reflections	7978 [R_{int} = 0.0855]
Completeness to 2θ = 60.42°	100.0 %
Absorption correction	Multi-scan
Maximum and minimum transmission	0.4932 and 0.4028
Refinement method	Full-matrix least-squares on F^2
Data / restraints / parameters	7978 / 0 / 355
Goodness-of-fit on F^2[a]	1.010
Final R indices [$I > 2\sigma(I)$][b]	R_1 = 4.69 %, wR_2 = 9.00 %
R indices (all data)	R_1 = 9.26 %, wR_2 = 10.48 %
Largest diff. peak and hole	0.72 and –0.69 e.Å^{-3}

[a] GooF = $[\Sigma[w(F_o^2-F_c^2)^2] / (n-p)]^{1/2}$ where n is the number of reflections and p is the total number of parameters refined. [b] $R1 = \Sigma||F_o|-|F_c|| / \Sigma|F_o|$; $wR2 = [\Sigma[w(F_o^2-F_c^2)^2] / \Sigma[w(F_o^2)^2]]^{1/2}$

Table S3 | Crystallographic information for the structural refinement of **3**.

Empirical Formula	$SnMnN_6C_{54}BH_{49}$
Formula weight	966.43 g/mol
Temperature	100.0 K
Wavelength	0.71073 Å
Crystal System	Trigonal
Space Group	$R\bar{3}$
Unit Cell Dimensions	a = 12.3824(6) Å, α = 90.0° b = 12.3824(6) Å, β = 120.0° c = 49.104(2) Å, γ = 90.0°
Volume	6520.2(7) Å^3
Z	6
Density (calculated)	1.477 g/cm^3
Absorption coefficient	0.912 mm^{-1}
F_{000}	2970.0
Crystal color	Colorless
Crystal size	0.456 × 0.419 × 0.110 mm^3
2θ range	3.888 to 60.114°
Index ranges	$-17 \le h \le 17$ $-17 \le k \le 16$ $-69 \le l \le 69$
Reflections collected	55305
Independent reflections	4263 [R_{int} = 0.0425]
Completeness to 2θ = 60.114°	100.0 %
Absorption correction	Multi-scan
Maximum and minimum transmission	0.9927 and 0.7230
Refinement method	Full-matrix least-squares on F^2
Data / restraints / parameters	4263 / 0 / 173
Goodness-of-fit on F^2[a]	1.048
Final R indices [$I > 2\sigma(I)$][b]	R_1 = 5.33 %, wR_2 = 14.90 %
R indices (all data)	R_1 = 6.53 %, wR_2 = 16.47 %
Largest diff. peak and hole	5.01 and –1.62 e.Å^{-3}

[a] GooF = $[\Sigma[w(F_o^2-F_c^2)^2] / (n-p)]^{1/2}$ where n is the number of reflections and p is the total number of parameters refined. [b] $R1 = \Sigma||F_o|-|F_c|| / \Sigma|F_o|$; $wR2 = [\Sigma[w(F_o^2-F_c^2)^2] / \Sigma[w(F_o^2)^2]]^{1/2}$

Table S4 | Crystallographic information for the structural refinement of **4**.

Empirical Formula	$SnFeN_6C_{54}BH_{49}$
Formula weight	967.34 g/mol
Temperature	100.0 K
Wavelength	0.71073 Å
Crystal System	Trigonal
Space Group	$R\bar{3}$
Unit Cell Dimensions	a = 12.3722(2) Å, α = 90.0° b = 12.3722(2) Å, β = 120.0° c = 48.796(1) Å, γ = 90.0°
Volume	6468.6(2) Å^3
Z	6
Density (calculated)	1.490 g/cm^3
Absorption coefficient	0.962 mm^{-1}
F_{000}	2976.0
Crystal color	Orange
Crystal size	0.127 × 0.056 × 0.025 mm^3
2θ range	2.504 to 60.128°
Index ranges	$-16 \le h \le 15$ $-17 \le k \le 17$ $-68 \le l \le 68$
Reflections collected	37148
Independent reflections	4228 [R_{int} = 0.0295]
Completeness to θ = 60.128°	100.0 %
Absorption correction	Multi-scan
Maximum and minimum transmission	0.9879 and 0.8782
Refinement method	Full-matrix least-squares on F^2
Data / restraints / parameters	4228 / 0 / 173
Goodness-of-fit on F^2[a]	1.049
Final R indices [I > 2σ(I) = 10408 data][b]	R_1 = 3.03 %, wR_2 = 7.06 %
R indices (all data, 0.80 Å)	R_1 = 4.15 %, wR_2 = 7.71 %
Largest diff. peak and hole	0.39 and –0.91 e.Å^{-3}

[a] GooF = $[\Sigma[w(F_o^2-F_c^2)^2] / (n-p)]^{1/2}$ where n is the number of reflections and p is the total number of parameters refined. [b] $R1 = \Sigma||F_o|-|F_c|| / \Sigma|F_o|$; $wR2 = [\Sigma[w(F_o^2-F_c^2)^2] / \Sigma[w(F_o^2)^2]]^{1/2}$

Table S5 | Crystallographic information for the structural refinement of **6**.

Empirical Formula	$SnNiN_6C_{54}BH_{49}$
Formula weight	970.20 g/mol
Temperature	100.0 K
Wavelength	0.71073 Å
Crystal System	Trigonal
Space Group	*R*–3
Unit Cell Dimensions	a = 12.3186(4) Å, α = 90.0°
	b = 12.3186(4) Å, β = 120.0°
	c = 49.082(2) Å, γ = 90.0°
Volume	6450.4(5) Å^3
Z	6
Density (calculated)	1.499 g/cm^3
Absorption coefficient	1.066 mm^{-1}
F_{000}	2988.0
Crystal color	Turquoise
Crystal size	0.443 × 0.380 × 0.044 mm^3
2θ range	2.49 to 61.21°
Index ranges	$-17 \le h \le 17$
	$-17 \le k \le 17$
	$-70 \le l \le 69$
Reflections collected	65036
Independent reflections	4430 [R_{int} = 0.0329]
Completeness to θ = 52.48°	100.0 %
Absorption correction	Multi-scan
Maximum and minimum transmission	0.8872 and 0.6505
Refinement method	Full-matrix least-squares on F^2
Data / restraints / parameters	4430 / 0 / 173
Goodness-of-fit on F^2[a]	1.050
Final *R* indices [I > 2σ(I) = 10408 data][b]	R_1 = 3.27 %, wR_2 = 8.23 %
R indices (all data, 0.80 Å)	R_1 = 4.15 %, wR_2 = 8.71 %
Largest diff. peak and hole	0.60 and –0.90 e.Å^{-3}

[a] GooF = $[\Sigma[w(F_o^2-F_c^2)^2] / (n-p)]^{1/2}$ where n is the number of reflections and p is the total number of parameters refined. [b] $R1 = \Sigma||F_o|-|F_c|| / \Sigma|F_o|$; $wR2 = [\Sigma[w(F_o^2-F_c^2)^2] / \Sigma[w(F_o^2)^2]]^{1/2}$

Table S6 | Crystallographic information for the structural refinement of **7**.

Empirical Formula	$SnZnN_6C_{54}BH_{49}$
Formula weight	976.86 g/mol
Temperature	100.0 K
Wavelength	0.71073 Å
Crystal System	Monoclinic
Space Group	*R*–3
Unit Cell Dimensions	a = 12.3859(4) Å, α = 90.0°
	b = 12.3859(4) Å, β = 120.0°
	c = 48.738(2) Å, γ = 90.0°
Volume	6475.2(5) Å^3
Z	6
Density (calculated)	1.503 g/cm^3
Absorption coefficient	1.181 mm^{-1}
F_{000}	3000.0
Crystal color	Colorless
Crystal size	0.470 × 0.260 × 0.044 mm^3
2θ range	3.888 to 58.378°
Index ranges	$-16 \le h \le 16$
	$-16 \le k \le 16$
	$-66 \le l \le 66$
Reflections collected	54021
Independent reflections	3891 [R_{int} = 0.0448]
Completeness to θ = 58.378°	99.96 %
Absorption correction	Multi-scan
Maximum and minimum transmission	0.9514 and 0.7101
Refinement method	Full-matrix least-squares on F^2
Data / restraints / parameters	3891 / 0 / 173
Goodness-of-fit on F^2[a]	1.088
Final *R* indices [I > 2σ(I) = 10408 data][b]	R_1 = 4.22 %, wR_2 = 10.96 %
R indices (all data, 0.80 Å)	R_1 = 5.01 %, wR_2 = 11.72 %
Largest diff. peak and hole	2.48 and –1.62 e.Å^{-3}

[a] GooF = $[\Sigma[w(F_o^2-F_c^2)^2] / (n-p)]^{1/2}$ where n is the number of reflections and p is the total number of parameters refined. [b] $R1 = \Sigma||F_o|-|F_c|| / \Sigma|F_o|$; $wR2 = [\Sigma[w(F_o^2-F_c^2)^2] / \Sigma[w(F_o^2)^2]]^{1/2}$

Table S7 | Comparison of ^{57}Fe Mössbauer parameters between compound **4** and known values of similar compounds.

Compound	δ (mm s^{-1})	ΔE_Q (mm s^{-1})
^{Ph,Me}TpFeSnPh$_3$ (**4**)	0.742(1)	1.061(3)
PhB(MesIm)$_3$Fe–N=PPh$_3$[32]	0.44(1)	0.78(1)
[PhBP$_3^{CH_2Cy}$]Fe–N=PPh$_3$[33]	0.820	1.449
[PhBP$_3^{iPr_3}$]Fe–N=PPh$_3$[33]	0.617	1.373

Table S8 | Fit parameters to the variable-temperature, variable field magnetization data of **3**, **4**, **5**, **6**. Parameters for **4** were reported previously[5], but are displayed here for easier comparison.

Compound	D (cm^{-1})	E (cm^{-1})	g_{iso}
3	−0.2(1)	0	1.99(2)
4	12.9(3)	3.3(2)	2.14(1)
5	11.9(1)	0.7(1)	2.28(2)
6	−3.0(2)	0	2.28(2)

Table S9 | Fit parameters to the cw-EPR spectra of samples of **1** and **3** diluted in a polycrystalline sample of **7** in a 1:20 (Mn:Zn) ratio.

Compound	Temperature (K)	g_{iso}	D (cm^{-1})	A_{iso} (^{55}Mn, MHz)	A_{iso} (^{nat}Sn, MHz)
1	298	1.999(2)	0.230(1)	-	-
	10	1.999(2)	0.236(1)	-	-
3	298	1.9933(2)	0.0939(4)	164(2)	141(3)
	12	1.9933(3)	0.1015(6)	164(3)	-

Table S10 | Results from peak-fitting XANES data at Sn K-edge for **3** – **7**, and SnO, SnO_2, Ph_6Sn_2, Ph_4Sn, Ph_3SnCl, and Ph_3SnF references. The step was fit with an arctangent function and the peaks were fit with pseudo-Voigt functions with $\gamma = 0.5$ for all compounds. Peak and step positions are reported in eV.

Compound	Step			Peak 1			Peak 2			Reduced
	Height	Center	Width	Height	Center	σ	Height	Center	σ	χ^2
3	0.847	29201.7	3.5	9.72	29209.1	18.09	0.701	29223.7	7.97	0.0047
4	0.829	29201.7	3.53	10.117	29209.1	18.24	0.828	29223.7	8.29	0.0049
5	0.830	29201.7	3.52	10.404	29208.7	18.84	0.779	29223.5	7.81	0.0055
6	0.829	29201.8	3.51	10.473	29208.7	18.85	0.85	29223.7	8.49	0.0056
7	0.771	29201.7	3.64	10.469	29209.1	17.20	2.62	29223.8	13.92	0.0051
Ph_6Sn_2	0.718	29201.0	1.59	9.272	29204.1	12.22	7.26	29224.5	22.58	0.0052
Ph_4Sn	0.719	29201.1	1.68	9.303	29204.1	12.10	7.29	29224.8	22.72	0.0057
Ph_3SnCl	0.749	29201.2	1.74	9.319	29204.1	12.02	7.27	29224.2	22.86	0.0099
Ph_3SnF	0.759	29202.1	2.21	9.704	29203.3	10.83	6.80	29225.0	24.30	0.0081
SnO	0.895	29200.1	4.73	10.796	29203.8	13.69	0.71	29215.4	7.66	0.0026
SnO_2	0.682	29203.4	5.18	14.65	29208.7	13.15	3.39	29224.6	13.16	0.0099

Table S11 | Fit parameters to the ^{119}Sn synchrotron Mössbauer spectra of polycrystalline samples of **4** – **7** at 60 K.

Compound	ΔE_Q (mm s^{-1})	χ^2
3	0.623(3)	2.54
4	1.198(2)	2.08
5	1.204(4)	2.11
6	1.134(2)	1.99
7	0.896(2)	2.58

Table S12 | Charges computed using the intrinsic bond orbital (IBO) charge localization from the TPSSh calculation. Note that N1 refers to nitrogen coordinated to the transition metal (TM) while N2 refers to the nitrogen coordination to boron.

Atom	3	4	5	6	7
Sn	0.266	0.320	0.365	0.263	-0.530
TM	1.154	1.077	1.017	1.042	3.755
B	0.081	0.082	0.071	0.088	-0.046
$N1_{avg}$	-0.352	-0.343	-0.339	-0.232	-0.472
$N2_{avg}$	-0.054	-0.051	-0.060	-0.050	-0.113

Table S13 | Atomic spin densities computed using the intrinsic bond orbital (IBO) charge localization from the TPSSh calculation. No spin density is included for Zn, since it is a closed shell singlet. The N atom designation is the same as in Table S12.

Atom	3	4	5	6
Sn	-0.006	0.060	0.130	-0.025
TM	4.764	3.672	2.583	1.688
B	0.001	0.001	0.002	0.000
$N1_{avg}$	0.041	0.058	0.064	0.066
$N2_{avg}$	0.002	-0.001	0.000	-0.004

Table S14 | Mayer and bond orders from the TPSSh and CASSCF calculations, respectively, analyzed using MultiWFN.

Compound	TPSSh	CASSCF
3	0.613	0.794
4	0.561	0.796
5	0.530	0.670
6	0.645	0.822
7	0.808	

Table S15 | Natural orbital occupation numbers for the σ bonding and antibonding orbitals from the CASSCF calculations. The effective bond order (EBO) computed using these occupation numbers is also reported.

Compound	Bonding	Antibonding	EBO
3	1.981	0.017	0.982
4	1.982	0.016	0.983
5	1.982	0.014	0.984
6	1.985	0.014	0.986

Table S16 | Contributions from Sn and the transition metal to the covalent sigma bond using IboView from the TPSSh calculation.

Compound	Sn	TM	Other Atoms
3	0.773	0.203	0.024
4	0.786	0.191	0.023
5	0.803	0.173	0.024
6	0.790	0.197	0.023
7	1.630	0.239	0.132

Table S17 | Percent contributions from Sn to each active space orbital using Hirshfeld method in MultiWFN from the CASSCF calculation.

	3	**4**	**5**	**6**
σ	54.58	52.54	50.59	49.27
$3d_{xy}$	0.48	0.46	0.43	0.36
$3d_{x^2-y^2}$	0.50	0.47	0.44	0.36
$3d_{z^2}$	1.45	1.77	2.96	3.40
$3d_{xz}$	1.67	1.66	1.57	1.27
$3d_{yz}$	1.67	1.67	1.57	1.27
σ*	34.38	32.11	26.38	30.06
$4d_{xy}$	1.95	2.08	2.80	1.87
$4d_{x^2-y^2}$	1.95	2.10	2.78	1.88
$4d_{z^2}$	8.48	10.94	16.32	11.19
$4d_{xz}$	9.31	9.17	9.06	5.85
$4d_{yz}$	9.31	9.17	9.05	5.85

Table S18 | Percent contributions from the transition metal to each active space orbital using Hirshfeld method in MultiWFN from the CASSCF calculation.

	3	**4**	**5**	**6**
σ	30.88	33.26	35.28	36.85
$3d_{xy}$	95.61	95.45	95.28	96.00
$3d_{x^2-y^2}$	95.61	95.45	95.28	96.00
$3d_{z^2}$	93.75	93.06	91.17	91.15
$3d_{xz}$	94.49	94.46	94.58	95.20
$3d_{yz}$	94.49	94.46	94.58	95.20
σ*	50.72	51.87	55.56	54.18
$4d_{xy}$	85.17	84.04	81.83	87.17
$4d_{x^2-y^2}$	85.17	84.04	81.83	87.17
$4d_{z^2}$	78.11	75.65	70.91	78.43
$4d_{xz}$	79.99	79.74	78.91	84.72
$4d_{yz}$	79.99	79.74	78.91	84.72

Table S19 | s/p/d orbital contributions from Sn and the transition metal (TM) to the σ bonding orbital from the CASSCF calculations.

Element	Orbital	**3**	**4**	**5**	**6**
Sn	s	20.37	17.99	19.25	16.74
	p	39.02	38.06	38.39	35.62
	d	0.68	0.78	0.79	0.8
TM	s	15.76	17.9	14.6	17.79
	p	14.74	15.32	14.9	15.21
	d	4.66	6.05	7.92	9.45

Table S20 | Calculated zero-field splitting parameters for **3** – **6** given in cm^{-1} from SO-CASPT2.

Compound	Transition Metal	*D*	*E*
3	Mn (SS-CASPT2)	0.08	0.0
4	Fe (SS-CASPT2)	34.3	1.1
5	Co (SS-CASPT2)	13.5	2.6
6	Ni (SS-CASPT2)	-11.4	0.4
	Ni (MS-CASPT2)	-12.9	2.3

Table S21 | Relative energies (cm^{-1}) of the lowest lying high spin states at the CASPT2 level of theory using an (10e, 12o), (9e, 12o), and (8e, 12o) active space at the CASPT2 level of theory for **4**, **5**, and **6** respectively. Dashes represent excitations not observed within the energy limits of the spectrometer.

$TpFeSnPh_3$ (**4**)		$TpCoSnPh_3$ (**5**)		$TpNiSnPh_3$ (**6**)	
CASPT2	Experiment	CASPT2	Experiment	CASPT2	Experiment
0		0		0	
5	-	1858	-	3788	-
396	-	1861	-	3797	-
4669	4871	3936	-	4059	4333
4669		4964	5959	6848	Not allowed
		4979		6866	
		9008	9308	9011	10256
		15758	14572	17868	14104
		15774		17871	
		16986	15452	19005	17261

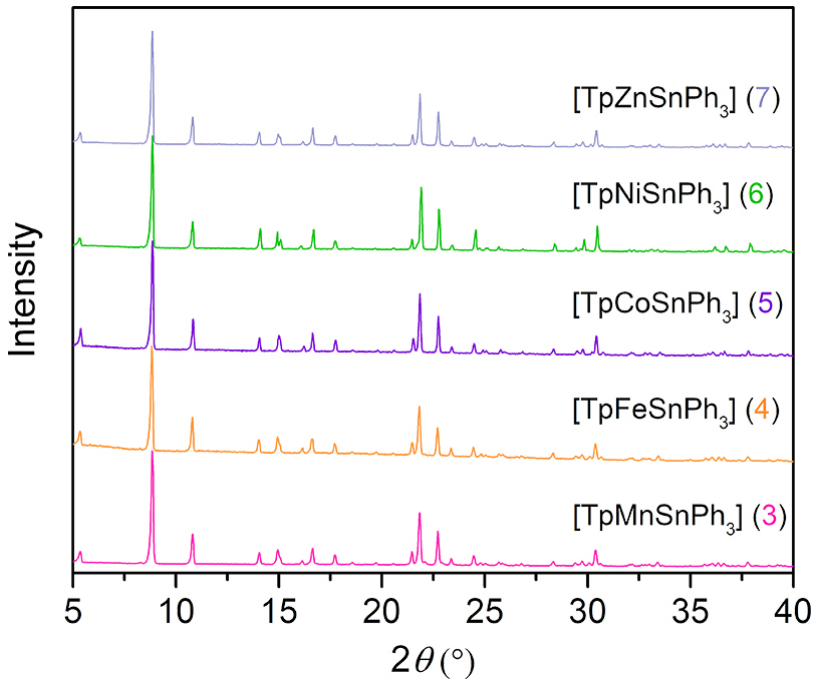

Figure S1 | Overlay of PXRD (CuKα1, λ = 1.5406 Å) patterns for **3** – **7** collected at room temperature under N_2.

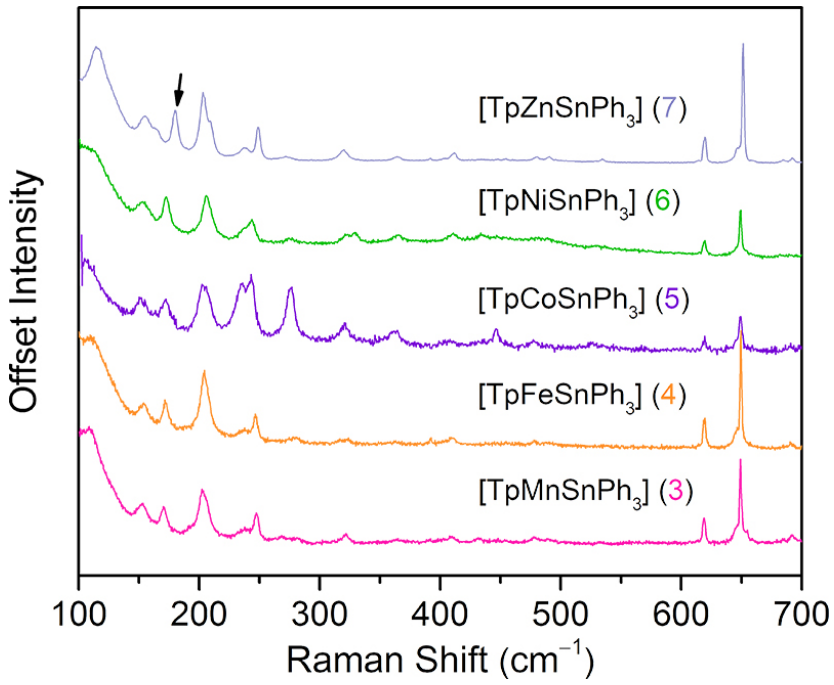

Figure S2 | Overlay of Raman spectra for **3** – **7** collected at room temperature under N_2. The black arrow highlights the TM-Sn bond stretching frequency.

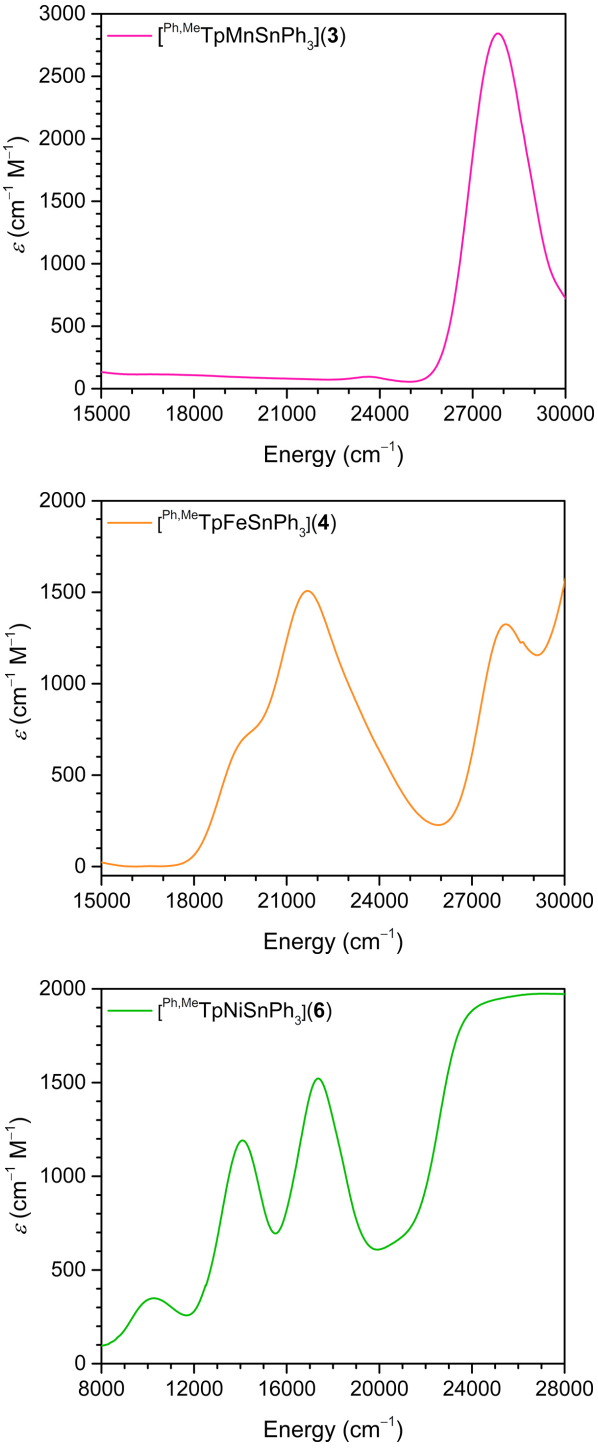

Figure S3 | Electronic absorption spectra of **3** (top), **4** (middle), and **6** (bottom) measured at room temperature in C_6D_6. Note: the peak at ~23,600 cm^{-1} in the spectrum of **3** is an artifact from background subtraction.

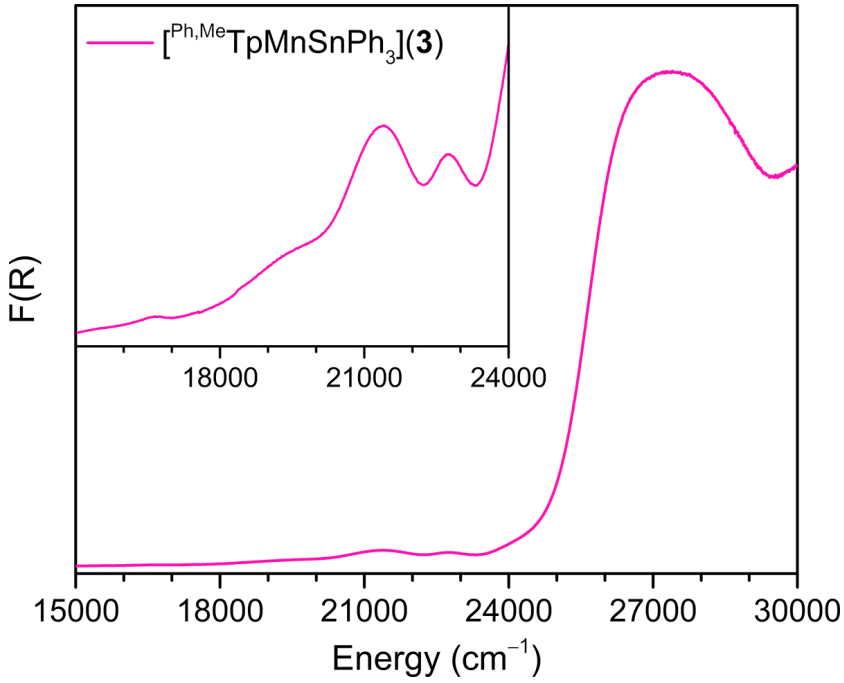

Figure S4 | Electronic absorption spectra of **3** measured at room temperature over KBr with an inset of the spectra magnified for easier visualization of the spin-forbidden transitions.

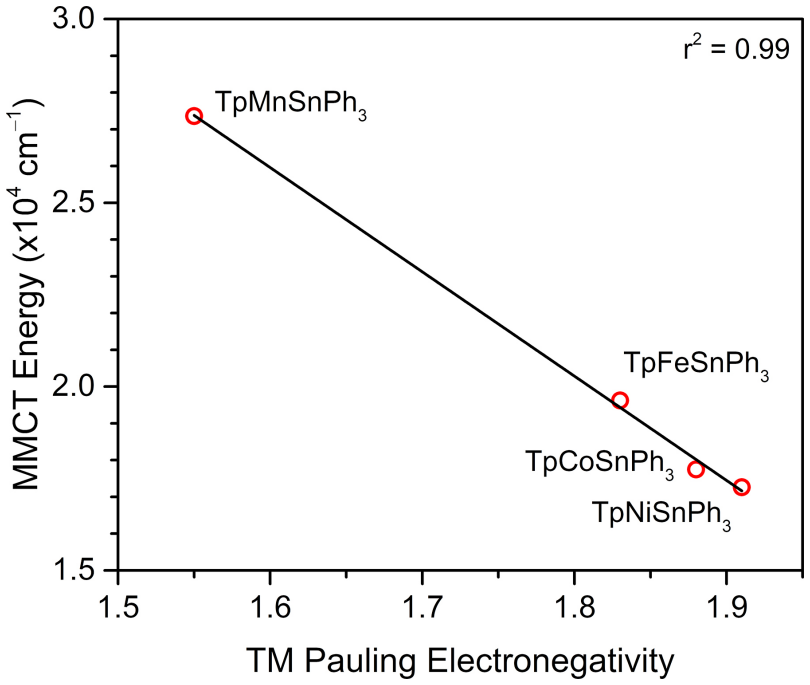

Figure S5 | Plot of metal-to-metal charge transfer band energy of **3** – **6** against transition metal (TM) Pauling electronegativity.

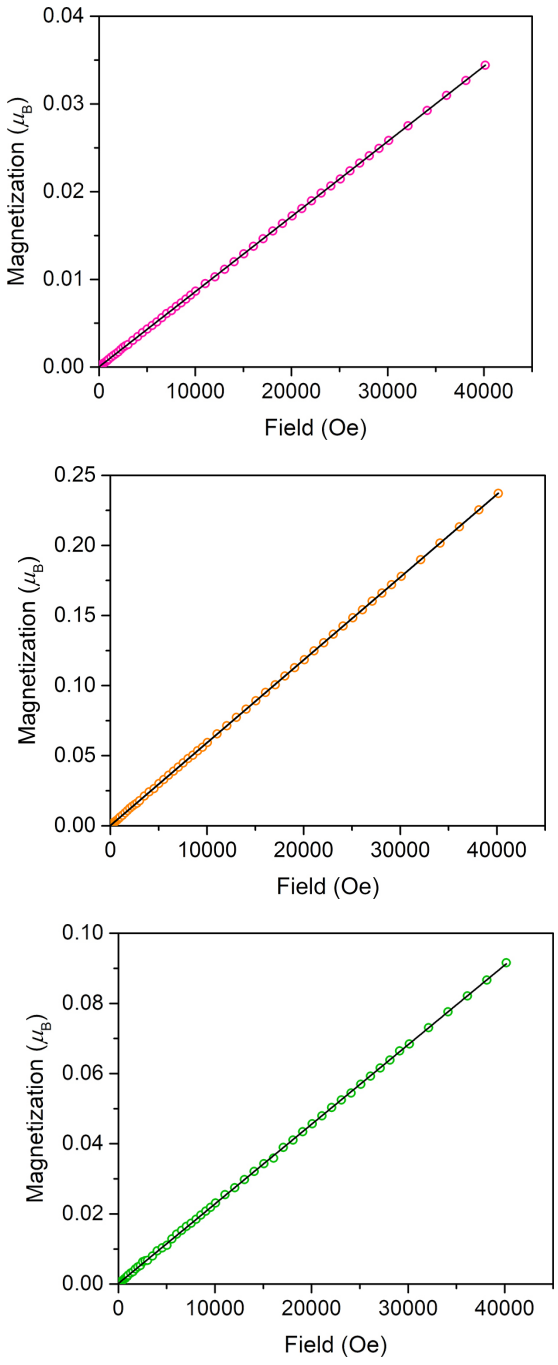

Figure S6 | Variable-field magnetization of polycrystalline samples of **3** (top), **4** (middle), **6** (bottom) restrained under eicosane acquired at 100 K. The black line is a linear fit to the data.

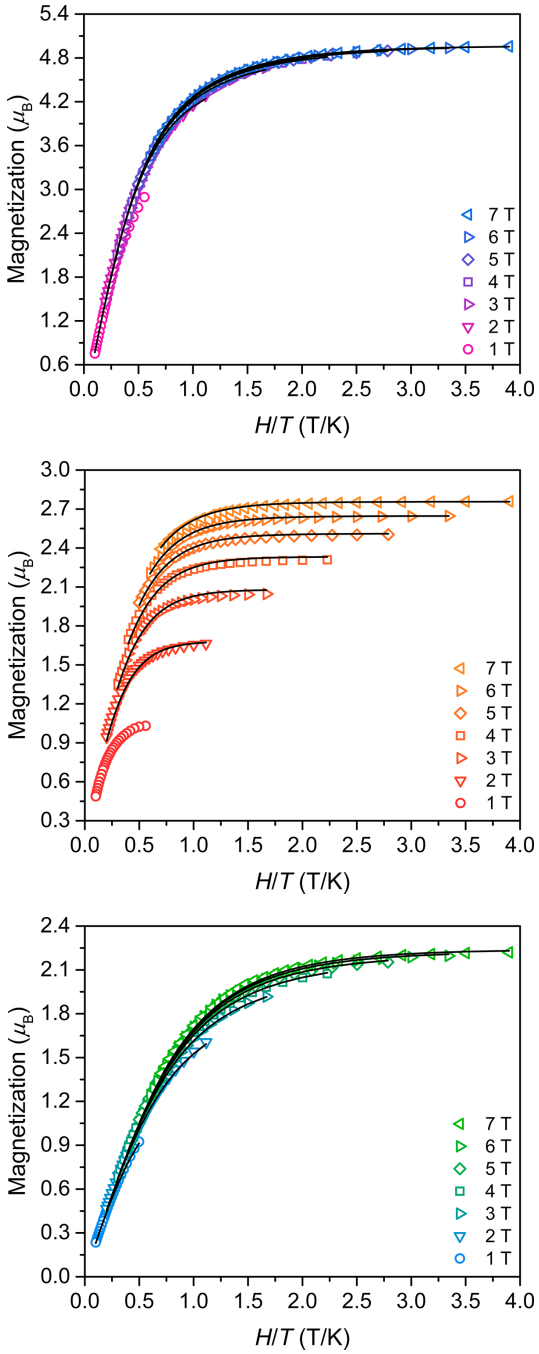

Figure S7| Variable-temperature, variable-field magnetization data for **3**, **4**, and **5** collected between 1.8 and 10 K from 1 to 7 T in 1 T increments. Black lines are simulations of the data obtained from fits using DAVE 2.0 and the spin Hamiltonian, $\hat{H} = g_{iso}\mu_B\mathbf{SH} + D[\hat{S}_z^2 - {}^1/_3S(S+1)]$**.** The parameters for the simulation are given in Table S8.

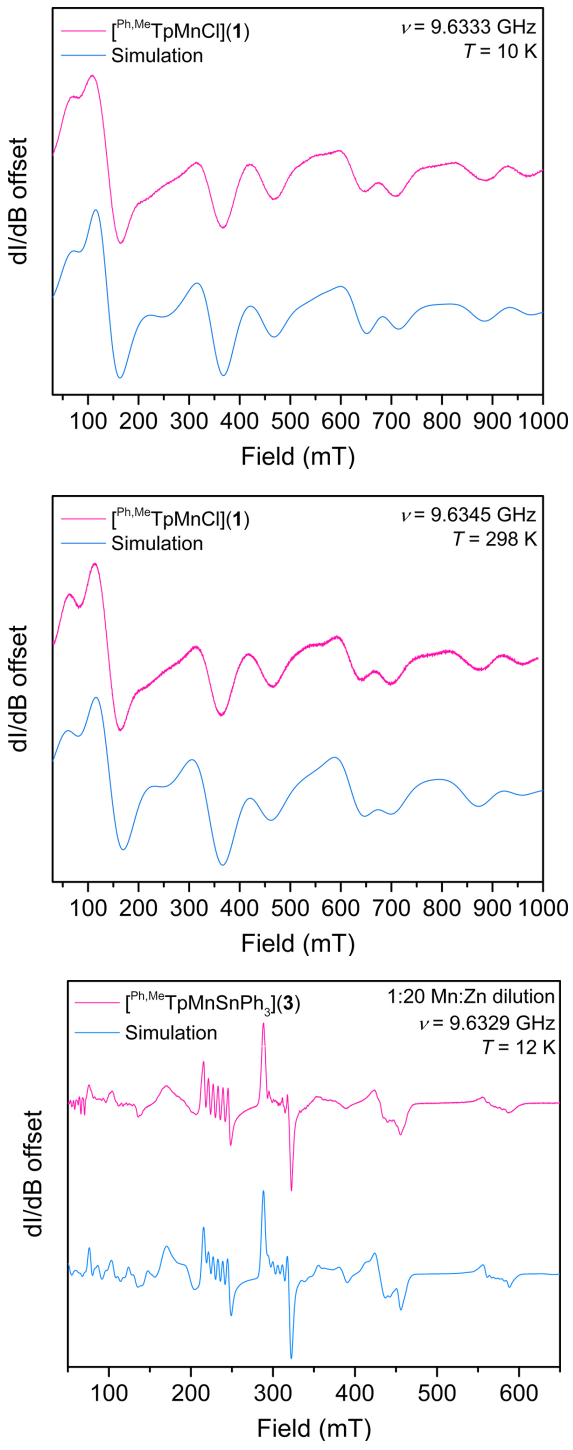

Figure S8| X-band cw-EPR spectrum of **1** (top and middle) and **3** (bottom) diluted in a polycrystalline sample of **7** in a 1:20 (Mn:Zn) ratio encased in eicosane. Simulations of the data were obtained from fits using Easyspin with the spin Hamiltonian, $\hat{H} = g_{iso}\mu_B\mathbf{SH} + \boldsymbol{AIS} + D[\hat{S}_z^2 - {}^1/_3S(S+1)]$. Parameters for the simulations are given in Table S9.

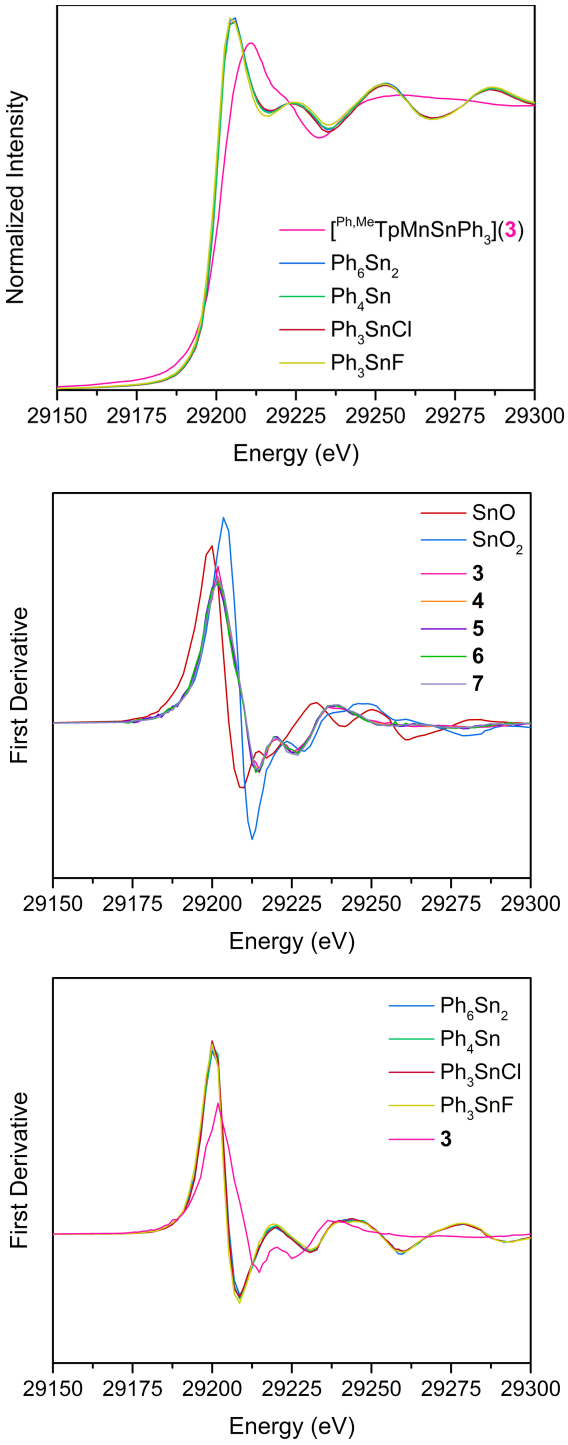

Figure S9 | (top) Overlay of XANES data at the Sn K-edge for powder samples of Ph_6Sn_2, Ph_4Sn, Ph_3SnCl, and Ph_3SnF, shown with the spectrum of **3** for reference, measured at 25 K. (middle) First derivative of XANES data for 3 – 7 with oxide references. (bottom) First derivative of XANES data for **3** and organometallic references.

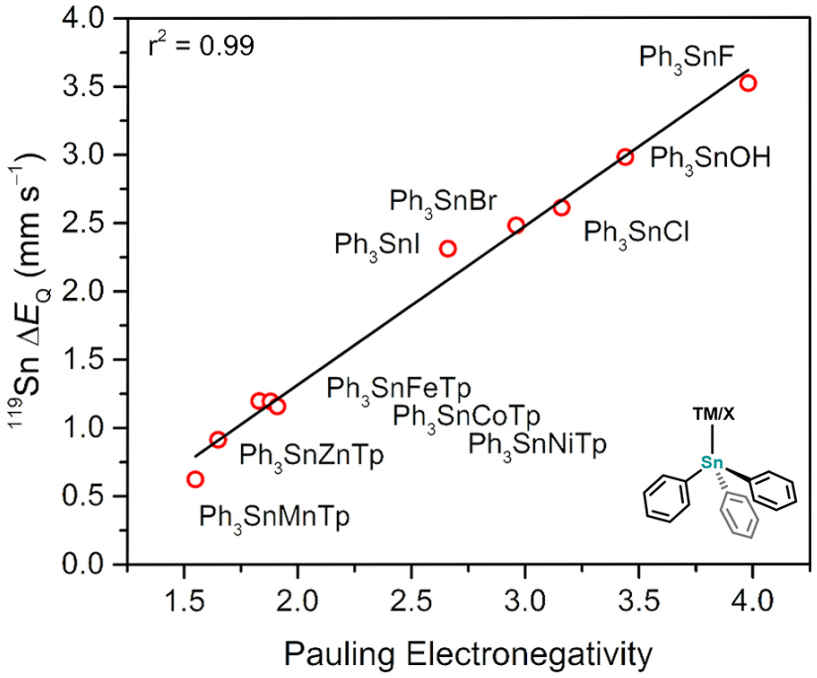

Figure S10 | Plot of ^{119}Sn ΔE_Q values of **3** – **7** (transition metal axial ligand, TM) and other triphenyl tin compounds (anionic axial ligand, X) against axial ligand Pauling electronegativity. ΔE_Q values for Ph_3SnX compounds taken from ref. 34.

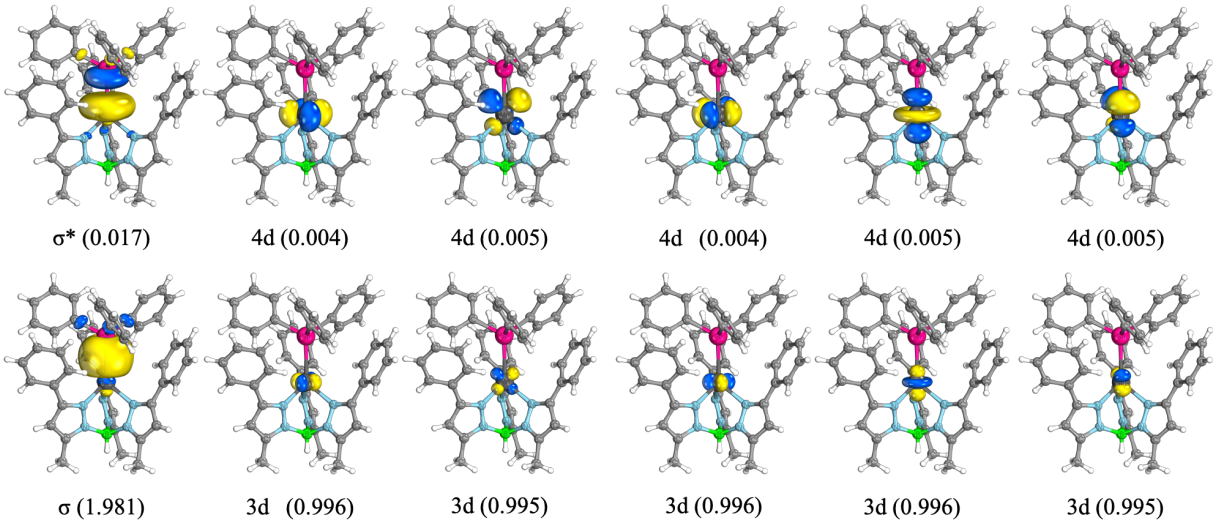

Figure S11 | Active natural orbitals from the SA1-CASSCF calculation of **3** in the sextet spin state. The corresponding occupation numbers from lowest CI Root are given in parentheses. An 80% threshold was used for plotting the orbitals.

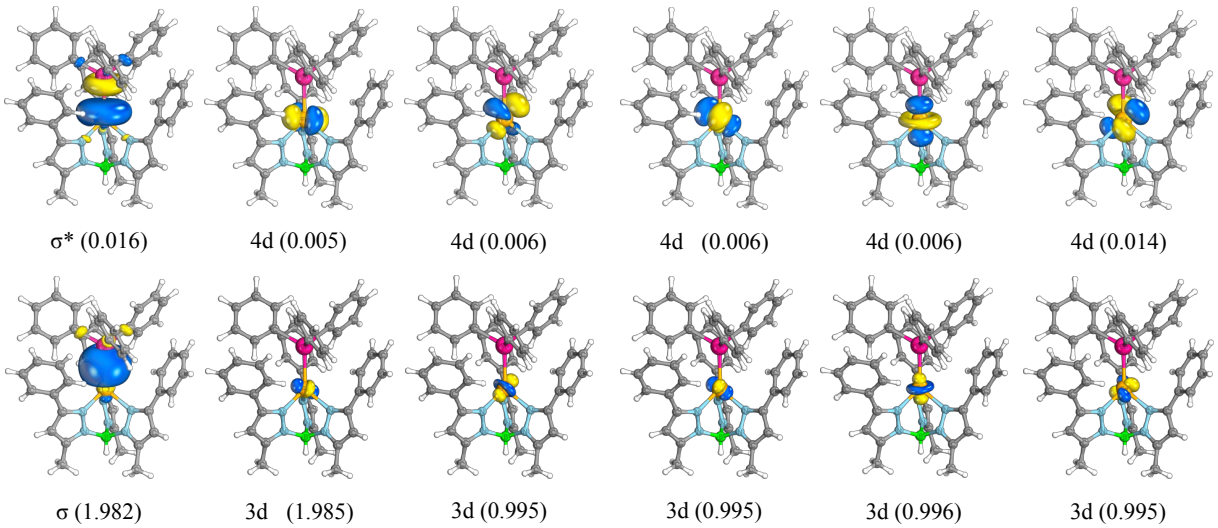

Figure S12 | Active natural orbitals from the SA5-CASSCF calculation of **4** in the quintet spin state. The corresponding occupation numbers from lowest CI Root are given in parentheses. An 80% threshold was used for plotting the orbitals.

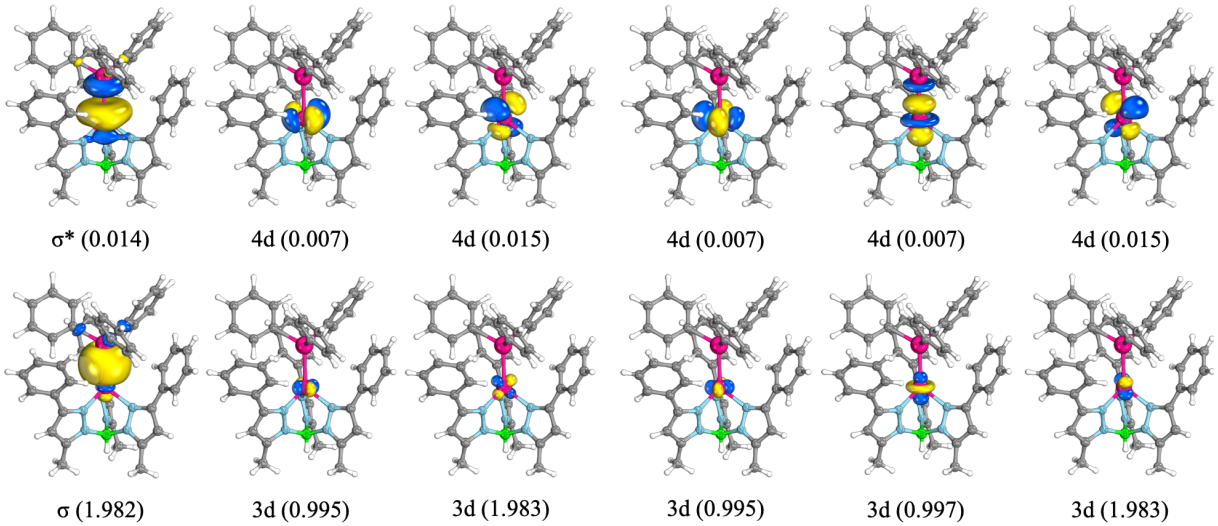

Figure S13 | Active natural orbitals from the SA10-CASSCF calculation of **5** in the quartet spin state. The corresponding occupation numbers from lowest CI Root are given in parentheses. An 80% threshold was used for plotting the orbitals.

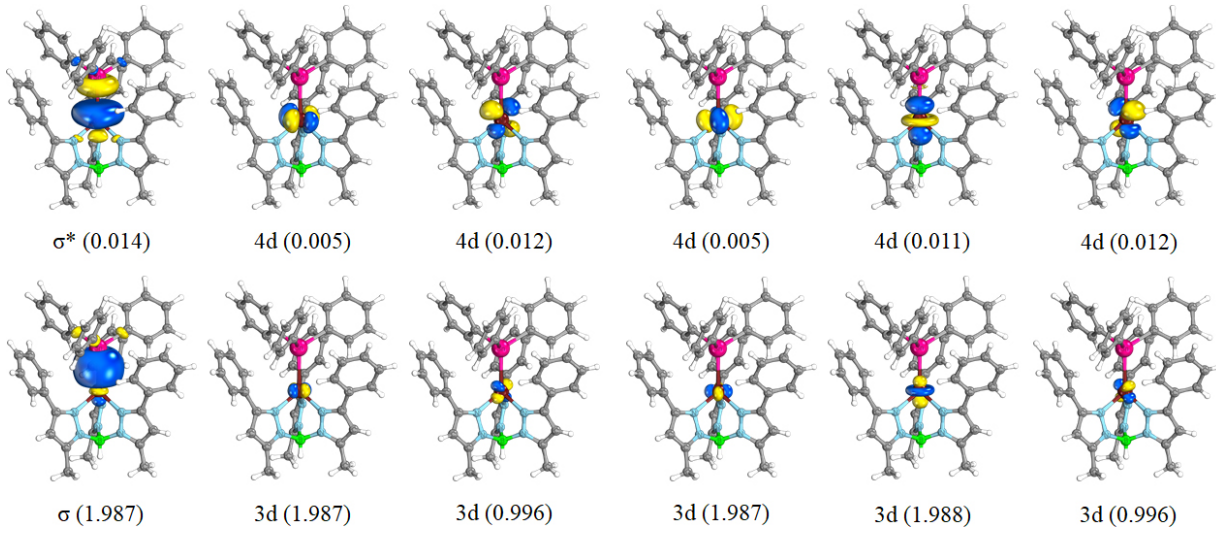

Figure S14 | Active natural orbitals from the SA10-CASSCF calculation of **6** in the triplet spin state. The corresponding occupation numbers from lowest CI Root are given in parentheses. An 80% threshold was used for plotting the orbitals.

References

1. D. T. Puerta and S. M. Cohen, *Inorg. Chim. Acta*, 2002, **337**, 459–462.
2. A. McSkimming and W. H. Harman, *J. Am. Chem. Soc.*, 2015, **137**, 8940–8943.
3. K. Uehara, S. Hikichi and M. Akita, *J. Chem. Soc., Dalton Trans.*, 2002, 3529–3538.
4. M. Abubekerov, T. L. Gianetti, A. Kunishita and J. Arnold, *Dalton Trans.*, 2013, **42**, 10525–10532.
5. S. C. Coste, T. J. Pearson and D. E. Freedman, *Inorg. Chem.*, 2019, **58**, 11893–11902.
6. G. A. Bain and J. F. Berry, *J. Chem. Educ.*, 2008, **85**, 532–536.
7. APEX3, v. 2017.3; Bruker Analytical X-ray Systems, Inc.: Madison, WI, 2017.
8. G. M. Sheldrick, SADABS, Version2.03; Bruker Analytical X-ray Systems, Inc.: Madison, WI, 2000.
9. G. M. Sheldrick, SHELXTL, Version 6.12; Bruker Analytical X-ray Systems, Inc.: Madison, WI, 2000.
10. L. J. Farrugia, *J. Appl. Cryst.* 1999, **32**, 837–838.
11. S. Stoll and A. Schweiger, *J. Magn. Reson.* 2006, **178**, 42–55.
12. B. Ravel and M. Newville, *J. Synchrotron Rad.*, 2005, **12**, 537–541.
13. TURBOMOLE V6.5 2013, a development of University of Karlsruhe and Forschungszentrum Karlsruhe GmbH, 1989-2007, TURBOMOLE GmbH, since 2007; available from http://www.turbomole.com.
14. J. M. Tao, J. P. Perdew, V. N. Staroverov, and G. E. Scuseria, *Phys. Rev. Lett.*, 2003**, 91,** 146401.
15. V. N. Staroverov, G. E. Scuseria, J. Tao and J. P. Perdew, *J. Chem. Phys.*, 2003, **119**, 12129. [Erratum] 2004, **121**, 11507(E).
16. F. Weigend, and F. Ahlrichs, *Phys. Chem. Chem. Phys*., 2005, **7**, 3297−3305.
17. K. Eichkorn, O. Treutler, H. Ohm, M. Haser and R. Ahlrichs, *Chem. Phys. Lett.*, 1995, **240**, 283–289.
18. K. Eichkorn, F. Weigend, O. Treutler and R. Ahlrichs, *Theor. Chem. Acc.*, 1997, **97**, 119–124.
19. M. Von Arnim, and R. Ahlrichs, *J. Comput. Chem.*, 1998, **19**, 1746–1757.
20. G. Knizia, *J. Chem. Theory Comput*., 2013, **9**, 4834–4843.
21. I. Mayer, *Chem. Phys. Lett*., 1983, **97**, 270−274.
22. T. Lu and F. Chen, *J. Comp. Chem*., 2012, **33**, 580−592.
23. B. O. Roos, P. R. Taylor and P. E. M. Siegbahn, *Chem. Phys.*, 1980, **48**, 157−173.
24. K. Andersson, P. Å. Malmqvist, B. O. Roos, A. J. Sadlej and K. Wolinski, *J. Phys. Chem.*, 1990, **94**, 5483−5488.
25. K. Andersson, P. Å. Malmqvist and B. O. Roos, *J. Chem. Phys.*, 1992, **96**, 1218−1226.
26. F. Aquilante, J. Autschbach, R. K. Carlson, L. F. Chibotaru, M. G. Delcey, L. De Vico, I. Fdez. Galván, N. Ferré, L. M. Frutos, L. Gagliardi, M. Garavelli, A. Giussani, C. E. Hoyer, G. Li Manni, H. Lischka, D. Ma, P. Å. Malmqvist, T. Müller, A. Nenov, M. Olivucci, T. B. Pedersen, D. Peng, F. Plasser, B. Pritchard, M. Reiher, I. Rivalta, I. Schapiro, J. Segarra-Martí, M. Stenrup, D. G. Truhlar, L. Ungur, A. Valentini, S. Vancoillie, V. Veryazov, V. P. Vysotskiy, O. Weingart, F. Zapata and R. Lindh, *J. Comput. Chem.*, 2016, **37**, 506−541.
27. M. Douglas and N. M. Kroll, *Ann. Phys.*, 1974, **82**, 89−155.
28. B. Hess, *Phys. Rev. A*, 1986, **33**, 3742−3748.
29. B. O. Roos, R. Lindh, P. Å. Malmqvist, V. Veryazov and P.-O. Widmark, *J. Phys. Chem. A*, 2004, **108**, 2851−2858.

30. B. O. Roos, R. Lindh, P. Å. Malmqvist, V. Veryazov and P.-O. Widmark, *J. Phys. Chem. A*, 2005, **109**, 6575−6579.
31. F. Aquilante, T. B. Pedersen and R. Lindh, *J. Chem. Phys*., 2007, **126**, 194106.
32. J. J. Scepaniak, T. D. Harris, C. S. Vogel, J. Sutter, K. Meyer and J. M. Smith, *J. Am. Chem. Soc.*, 2011, **133**, 3824–3827.
33. S. E. Creutz and J. C. Peters, *Inorg. Chem.*, 2016, **55**, 3894–3906.
34. R. C. Poller and J. N. R. Ruddick, *J. Organomet. Chem.*, 1972, **39**, 121−128.